

# Vector-Vector scattering at the LHC with two charged leptons and two neutrinos in the final state.

---

Alessandro Ballestrero<sup>a</sup>, Diogo Buarque Franzosi<sup>a,b</sup> and Ezio Maina<sup>a,b</sup>

<sup>a</sup> INFN, Sezione di Torino, Italy,

Via Giuria 1, 10125 Torino, Italy,

<sup>b</sup> Dipartimento di Fisica Teorica, Università di Torino, Italy

Via Giuria 1, 10125 Torino, Italy.

Email: ballestrero@to.infn.it, buarque@to.infn.it, maina@to.infn.it.

ABSTRACT: A complete parton level analysis of  $2\ell 2\nu 2j$  and  $4\ell 2j$ ,  $\ell = \mu, e$  production at the LHC is presented, including all processes at order  $\mathcal{O}(\alpha_{EM}^6)$ ,  $\mathcal{O}(\alpha_{EM}^4 \alpha_S^2)$ . The infinite Higgs mass scenario, which is considered as a benchmark for strong scattering theories and is the limiting case for composite Higgs models, and one example of Strongly Interacting Light Higgs models are confronted with the Standard Model light Higgs predictions. This analysis is combined with the results in the  $\ell\nu + \text{four jets}$ , the  $\ell^-\ell^+ + \text{four jets}$  and the  $3\ell\nu + \text{two jets}$  channels presented in previous papers, in order to determine whether these alternative Higgs frameworks can be detected as an excess of events in boson–boson scattering.

---

## Contents

<b>1. Introduction</b>	<b>1</b>
<b>2. Calculation</b>	<b>3</b>
<b>3. The <math>2j\ell^\pm\ell'^\pm\nu\nu</math> channel: two same-sign leptons in the final state</b>	<b>6</b>
<b>4. The <math>2jZZ \rightarrow 2j\ell^+\ell^-\nu\bar{\nu}</math> channel: two opposite-sign same-flavour leptons in the final state</b>	<b>9</b>
<b>5. The <math>2jW^+W^- \rightarrow 2j\ell^+\ell^-\nu\bar{\nu}</math> channel: two opposite-sign leptons in the final state</b>	<b>11</b>
<b>6. The <math>2j4\ell</math> channel</b>	<b>13</b>
<b>7. Combining all channels</b>	<b>15</b>
<b>8. Conclusions</b>	<b>19</b>

---

## 1. Introduction

Whether or not the search for a light Higgs boson at the LHC will be successful, vector boson scattering processes will require careful analysis. In fact, the corresponding amplitudes involving only vector bosons grow with energy when the bosons are longitudinally polarized and violate perturbative unitarity at about one TeV, requiring either the Higgs or some new physics in the energy range accessible to the LHC in order to tame this unphysical behaviour<sup>1</sup>.

The Standard Model (SM) describes Electroweak Symmetry Breaking (EWSB) through a single complex Higgs doublet. Many alternative mechanisms of EWSB however have been explored. We will not try to summarize the different models and simply refer to the literature. We will only remark that it is conceivable that composite states are responsible for EWSB [7, 8, 9, 10, 11, 12, 13, 14] . These theories typically predict the presence of new states which, if light enough, could be observed at the LHC.

The effective field theory approach [15, 16, 14, 17] is a powerful method for treating the low energy dynamics of systems with broken symmetries. It provides a systematic expansion of the full unknown Lagrangian in terms of the fields which are relevant at scales much lower than the symmetry breaking scale.

---

<sup>1</sup>Detailed reviews and extensive bibliographies can be found in Refs. [1, 2, 3, 4, 5, 6]

In Ref. [14] it has been pointed out that, if EWSB is triggered by a light composite Higgs which is a pseudo-Goldstone boson related to some large scale strongly interacting dynamics, the growth with energy of the vector boson scattering amplitudes typical of Higgsless models might not be completely canceled by Higgs exchange diagrams but only slowed down. This kind of models have been called Strongly Interacting Light Higgs (SILH) models. Examples which fall into this class are for instance the Holographic Higgs [12], the Little Higgs of Ref. [13] and the Littlest Higgs [9].

In SILH models the leading low energy effects are described by two parameters (one responsible for a universal modification of all Higgs couplings, and the other one for a universal modification of Higgs couplings to fermions) characterized by the ratio  $v^2/f^2 = \xi$ , where  $v$  is the Higgs vacuum expectation value and  $f$  is the  $\sigma$ -model scale. The natural range of the  $\xi$  parameter is between  $\xi = 0$  and  $\xi = 1$  which correspond respectively to the limiting cases of the Standard Model and of technicolor theories. Because of the modified Higgs couplings, longitudinal gauge-boson scattering amplitudes violate unitarity at high energy, even in the presence of a light Higgs [14].

Scattering processes among vector bosons have been scrutinized since a long time [18]. In Ref. [19, 20] an analysis of  $\ell\nu + \text{four jets}$  and  $\ell^+\ell^- + \text{four jets}$  production at the LHC has been presented, with the limitation of taking into account only purely electroweak processes. Preliminary results concerning the inclusion of the  $\mathcal{O}(\alpha_{EM}^4\alpha_S^2)$  background, which include  $VV + 2j$  and top-antitop production have appeared in Ref. [21]. A preliminary analysis in the Equivalent Vector Boson Approximation of the observability of partial unitarization of longitudinal vector boson scattering in SILH models at the LHC can be found in Ref. [22]. In the last few years QCD corrections to boson-boson production via vector boson fusion [23] at the LHC have been computed and turn out to be below 10%. Recently, VBFNLO [24] a Monte Carlo program for vector boson fusion, double and triple vector boson production at NLO QCD accuracy, limited to the leptonic decays of vector bosons, has been released. Recently, the first results for the NLO corrections to  $W + 4j$  production have appeared [25]. New techniques which exploit the angular distribution of vector boson decay products to determine the ratio of longitudinal and transverse polarization have been proposed in [26].

In Ref. [27] a complete parton level analysis of  $\ell\nu + \text{four jets}$  production at the LHC, including all processes at order  $\mathcal{O}(\alpha_{EM}^6)$ ,  $\mathcal{O}(\alpha_{EM}^4\alpha_S^2)$  and  $\mathcal{O}(\alpha_{EM}^2\alpha_S^4)$  has been presented, comparing a typical SM light Higgs scenario with the Higgsless case. It was noted that the  $\mathcal{O}(\alpha_{EM}^2\alpha_S^4) W + 4j$  background is so large that the usual approach of comparing the number of events in the two scenarios at large invariant masses is useless. It was argued that the invariant mass distribution of the two central jets in the vector-vector scattering signal presents a peak corresponding to the decays of vector bosons while the background produced by  $\mathcal{O}(\alpha_{EM}^2\alpha_S^4) W + 4j$  processes is rather flat and therefore can be measured from the sidebands and subtracted, drastically decreasing the theoretical uncertainties.

In Ref. [28] the processes  $pp \rightarrow \ell^+\ell^- + 4j$  and  $pp \rightarrow 3\ell\nu + 2j$  have been studied along the lines introduced in Ref. [27]. The infinite mass Higgs scenario and the instance of SILH models described above have been compared with the light Higgs SM framework.

In this paper we concentrate on the boson boson scattering reactions which produce

a  $2\ell 2\nu 2j$  final state. Because of the presence of two neutrinos the mass of the final state boson pair cannot be reconstructed. For completeness sake in the end we also discuss the  $2j4\ell$  channel in which the vector pair mass can obviously be measured with high accuracy but which has been left out of our previous papers because of its small cross section. These processes have been studied already in Ref. [29] where they have been described as gold-plated. A potentially large background to these channels is the copious yield of high  $p_T$ , isolated leptons in B-hadron production [30] which mimic the signature of the leptonic decays of  $W$  bosons. A detailed experimental analysis of two same sign  $W$ 's has however shown that when standard isolation criteria are applied isolated leptons from B-hadrons can be efficiently eliminated [31]. Therefore, we have reanalyzed the  $2\ell 2\nu 2j$  channels using complete  $\mathcal{O}(\alpha_{EM}^6)$  and  $\mathcal{O}(\alpha_{EM}^4\alpha_S^2)$  samples.

We have estimated the probability that, assuming that either the Higgsless scenario or the instance of SILH model we have considered is realized in Nature, the results of the measurements at the LHC yield results which are incompatible with the SM. We have first combined separately the three channels,  $2j\ell^\pm\ell^\pm\nu\nu$ ,  $2jZZ \rightarrow 2j\ell\nu\ell\nu$ ,  $2jWW \rightarrow 2j\ell\nu\ell\nu$  in which the invariant mass of the final state cannot be directly measured and the four channel,  $2j4\ell$ ,  $4j\ell\nu, 4j\ell\ell$  and  $2j3\ell\nu$  in which it can instead be reconstructed. Finally we have combined all channels.

## 2. Calculation

Two perturbative orders contribute to  $2\ell 2\nu 2j$  and  $4\ell 2j$  at the LHC. The purely electroweak set of diagrams at  $\mathcal{O}(\alpha_{EM}^6)$  is the one which includes boson boson scattering as a subprocess. In the second set of diagrams at  $\mathcal{O}(\alpha_{EM}^4\alpha_S^2)$  no such scattering takes place: either two fermion lines exchange a gluon or a single fermion line and two external gluons are present.

Both the  $\mathcal{O}(\alpha_{EM}^6)$  and the  $\mathcal{O}(\alpha_{EM}^4\alpha_S^2)$  samples have been generated with PHANTOM, a dedicated tree level Monte Carlo generator which is documented in Ref. [32] while additional material can be found in Refs. [33, 34, 35]. The program generates events in the Les Houches Accord File Format [36]. In all samples full  $2 \rightarrow 6$  matrix elements, without any production times decay approximation, have been used. For the LHC we have assumed the design energy of 14 TeV. For each perturbative order we have generated a sample of five hundred thousand unweighted events. In some cases additional event samples have been generated in order to increase the final statistics of particular phase space regions.

All samples have been generated using CTEQ5L [37] parton distribution functions. The QCD scale has been taken as

$$\Lambda^2 = M_W^2 + \frac{1}{6} \sum_{i=1}^6 p_{Ti}^2 \quad (2.1)$$

in all cases but for the reaction in which a triplet of final state particles with flavours compatible with deriving from the decay of a top or antitop quark could be found. In this case the scale has been taken as

$$\Lambda^2 = M_{top}^2 + p_{Ttop}^2. \quad (2.2)$$

The analysis has been performed at parton level with no showering and hadronization.

The effective Lagrangian approach to SILH models of Ref. [14] is valid for small values of  $\xi$ , while larger values demand a more detailed description of the particular model at hand. Such a Lagrangian leads to a modification of the Higgs couplings by a factor  $1/\sqrt{1 + c_H\xi}$ , which can be reabsorbed in a Higgs propagator modification by a factor  $1/(1 + c_H\xi)$  in boson boson scattering studies.  $c_H$  is a pure number of order unity [9, 12, 13, 14]. For the present study we have selected the value  $c_H\xi = 1$  which we intend as a possible upper limit for the model independent lagrangian description of Ref. [14]. Both for the SM scenario and for the SILH model the Higgs mass has been fixed at 200 GeV. Since we are interested in large invariant mass vector vector scattering processes the actual value of the Higgs mass is irrelevant, provided it is appreciably smaller than the invariant mass of the vector pair.

For very large Higgs masses, all Born diagrams with Higgs propagators become completely negligible in the Unitary Gauge we work in. Therefore the no-Higgs model results for all processes coincide with those in the  $M_H \rightarrow \infty$  limit. This framework therefore can be considered as an upper limit to SILH models and also as representative of all models in which resonances which unitarize vector vector scattering are present but too heavy to be directly detected. Therefore the possibility of distinguishing the no-Higgs case from the SM at the LHC represent a benchmark for the observability of unitarized models. We postpone the discussion of these issues to Ref. [38].

In contrast with the processes examined in Refs. [27, 28] where the dominating background is due to  $V + 4j$   $\mathcal{O}(\alpha_{EM}^2\alpha_S^4)$  processes in which only one vector boson is produced, in the present case the final states from both perturbative orders contain two vector bosons and are essentially impossible to separate. The selection of events with jets widely separated in pseudorapidity is a well established technique for enhancing the scattering contributions at the LHC [18]. As shown in Ref. [27] a powerful tool to increase the separation between the SM predictions and those of the Higgsless scenario is provided, at large invariant masses, by the request that the vector bosons and their decay products are in the central part of the detector since the vector bosons in the Higgsless case have smaller rapidities and larger momenta than in the presence of a light Higgs.

The cuts in Tab. 1 have been applied either at generation level or as a preliminary step to any further analysis. They require containment within the active region of the detectors and minimum transverse momentum for all observed partons; a minimum mass separation is imposed for all same-family opposite-sign charged leptons and all jet pairs. Furthermore, the two jets are required to be separated by at least three ( $2j2\ell2\nu$ ) or four ( $2j4\ell$ ) units in rapidity and their combined mass is forced to be outside the electroweak vector boson mass window in order to exclude three vector boson production.

We have considered two different ranges for the mass of the lepton pair in the  $2j\ell^+\ell^-\nu\bar{\nu}$  channel. On one hand we have selected same flavour charged leptons with a mass in the interval  $76 \text{ GeV} < M(\ell^+\ell^-) < 106 \text{ GeV}$ . In this case we have considered the lepton pair to be produced in the decay of a  $Z$  boson. Requiring further a large missing transverse momentum we have produced an event sample corresponding to the  $2jZZ \rightarrow 2j\ell^+\ell^-\nu\bar{\nu}$  channel which will be discussed in Sect. 4. When the mass of the lepton pair is outside the quoted range or the two oppositely charged leptons belong to different families we consider

the event a candidate for the  $2jWW$  channel. Since we are interested into high invariant mass  $W$  pairs, we have required  $M(\ell^+\ell^-) > 250$  GeV for this kind of events which will be analyzed in Sect. 5. The mass of the  $WW$  system corresponds to the scale of boson boson scattering and large masses help in discriminating between the SM and other scenarios.

For both the Higgsless and SILH cases and for each channel we have computed the probability that, assuming a specific Beyond Standard Model (BSM) correctly describes nature, the result of an experimental outcome for a given luminosity has a chance of less than 5% in the SM (PBSM@95%CL).

For the combination of channels discussed in Sect. 7 we have also computed the 99.7% exclusion limit (PBSM@99.7%CL).

All limits presented in the following, unless explicitly mentioned, have been computed summing over all possible combinations of first and second generation leptons, assuming an integrated luminosity of  $L = 200 \text{ fb}^{-1}$ , which we intend as corresponding to one year of high luminosity combining CMS and ATLAS results.

We proceed as follows. For each channel we use as discriminant  $S$ , the sum of the events for all  $\mathcal{O}(\alpha_{EM}^6)$  and  $\mathcal{O}(\alpha_{EM}^4\alpha_S^2)$  processes after all selection cuts.  $S$  is considered as a random variable representing the number of signal events for a possible experimental outcome.  $\bar{S}$  is the corresponding average value which will be taken equal to the prediction of our simulation. We take into account the statistical uncertainty of  $S$  assuming a standard Poisson distribution with average  $\bar{S}$ . The predicted signal cross section is also affected by

theoretical uncertainties, so the parameter  $\bar{S}$  is itself subject to fluctuations. The theoretical error is modeled by a flat distribution in the window  $\bar{S} \pm 30\%$  which, in our opinion, is a reasonable choice to account for both pdf's and scale uncertainties for the signal. The processes we are interested in require center of mass energies of the order of the TeV and therefore involve quarks with rather large longitudinal momentum fraction  $x$ ,  $x \approx 10^{-1} \div 10^{-2}$  at a typical scale  $\Lambda$  of about 100 GeV. In this region the uncertainty due to the parton distribution functions is of the order of 5% [39, 40]. As already stated, QCD corrections are in the range of 10% and, as a consequence theoretical uncertainties are expected to be well within this order of magnitude.

Having computed the probability distributions  $P(S|SM)$  and  $P(S|BSM)$  of  $S$  in the Standard Model and in the Beyond the Standard Model under consideration, the 95%CL region for the SM can be defined from the probability ratio

$$Q(S) = \frac{P(S|BSM)}{P(S|SM)} \quad (2.3)$$

$p_T(\ell^\pm) > 20 \text{ GeV}$
$ \eta(\ell^\pm)  < 3.0$
$M(\ell^+\ell^-) > 20 \text{ GeV}$
$M(\ell^+\ell^-) > 250 \text{ GeV} \quad (2jW^+W^-)$
$76 \text{ GeV} < M(\ell^+\ell^-) < 106 \text{ GeV} \quad (2jZZ)$
$p_T(j) > 30 \text{ GeV}$
$ \eta(j)  < 6.5$
$M(jj) > 60 \text{ GeV}$
$M(jj) < 70 \text{ GeV}; M(jj) > 100 \text{ GeV}$
$ \Delta\eta(jj)  > 3.0 \quad (2j2\ell2\nu)$
$ \Delta\eta(jj)  > 4.0 \quad (2j4\ell)$

**Table 1:** Acceptance cuts.

determining a number  $\alpha$  such that

$$\int dS P(S|SM) \theta(\alpha - Q) = 95\%. \quad (2.4)$$

The probability for the BSM to yield a result outside this 95%CL region for the SM is then

$$P_{BSM@95\%CL} = \int dS P(S|BSM) \theta(Q - \alpha). \quad (2.5)$$

A number of comments, which apply to all channels discussed in this paper, should be made. We have performed a simple cut based study, which can undoubtedly be improved upon with a more sophisticated multivariate analysis. On the other hand we have not taken into account experimental efficiencies and all issues related to additional hadronic activity due to showering and the underlying event. The selection cuts discussed below have been chosen in order to maximize the separation of the light Higgs case from the no-Higgs one.

In the following we will present cross sections as a function of appropriate minimum invariant masses  $M_{cut}$ , typically extracted from lepton momenta. The best discrimination between the SM and the BSM schemes are generally obtained for  $M_{cut}$  values which yield production rates which are uncomfortably small, particularly because of neglected experimental uncertainties. It should however be noticed that at smaller values of  $M_{cut}$  the rate is usually much larger with a modest decrease of discriminating power.

### 3. The $2j\ell^\pm\ell'^\pm\nu\nu$ channel: two same-sign leptons in the final state

This channel, which is characterized by two same sign charged leptons, possibly of different flavour, in the final state, has low EW and QCD background, for no external gluons contribute to this final state. We remark that the production of two same-sign  $W$ 's has been extensively discussed in the context of Multiple Particle Interactions (MPI) [41, 42, 43], since it has the peculiarity that it can be realized in MPI at a lower perturbative order than in ordinary two parton collisions where at least two additional partons must appear in the final state. However, if two jets in the final state are required, the MPI contribution is small and concentrated in the region of small total visible energy and therefore has been neglected.

The presence of two neutrinos in the final state makes it impossible to reconstruct the invariant mass of the di-boson system which corresponds to the center of mass energy of the  $WW$  scattering. For  $M_{cut}$  we have resorted to a correlated observable, the di-lepton mass  $M(\ell\ell)$ .

The total cross section for the  $2j\ell^\pm\ell'^\pm\nu\nu$  channel with the acceptance cuts in Tab. 1 is presented in Tab. 2 as a function of the minimum  $\ell\ell$  invariant mass  $M_{cut}$ . In parentheses the results for the  $\mathcal{O}(\alpha_{EM}^6)$  processes. Tab. 2 shows that the cross section for the  $\mathcal{O}(\alpha_{EM}^4\alpha_S^2)$  processes is only about 25% to 40% of the total cross section in the Higgsless scenario already at this level. The distribution of the lepton pair mass, with acceptance cuts only, is presented on the left hand side of Fig. 1. The  $\mathcal{O}(\alpha_{EM}^4\alpha_S^2)$  background is negligible at

$M_{cut}$ (GeV)	no Higgs	SILH	$M_H = 200$ GeV
	$\sigma$ (fb)	$\sigma$ (fb)	$\sigma$ (fb)
200	3.11(2.39)	2.87(2.15)	2.73(2.01)
300	1.73(1.23)	1.55(1.06)	1.46(.967)
400	1.01(.682)	.892(.560)	.839(.507)
500	.630(.407)	.538(.315)	.505(.283)
600	.400(.253)	.334(.187)	.311(.163)
700	.262(.162)	.214(.114)	.198(.0975)
800	.177(.108)	.142(.0728)	.130(.0613)

**Table 2:** Total cross section for the  $\ell^\pm\ell^\pm\nu\nu + 2j$  channel after generation cuts, Tab. 1. In parentheses the results for the  $\mathcal{O}(\alpha_{EM}^6)$  sample.

small di-lepton mass, while it becomes of the same order of magnitude of the  $\mathcal{O}(\alpha_{EM}^6)$  contribution for  $M_{cut} > 500$  GeV.

In the following, as already mentioned, we will consider the full sample as our signal. It is possible to improve the discriminating power of the analysis increasing the fraction of  $\mathcal{O}(\alpha_{EM}^6)$  events in the event sample since only those are sensitive to the mechanism of EWSB. Therefore, on the generated samples we have applied the additional selection cuts shown in Tab. 3. These cuts force the two tag jets to be well separated and not central. One of the two leading jets is forbidden from having a very large transverse momentum. The two charged leptons are required to be rather central and well separated from the jets. They are required to be well separated in the transverse plane and to have large transverse momentum. Finally, the vector difference between the lepton momenta is required to be large.

$\Delta\eta(jj) > 4.5$
$max \eta(j)  > 2.5$
$ \eta(j)  > 1.$
$ \eta(\ell)  < 2.5$
$p_T(\ell) > 50$ GeV
$minp_T(j) < 120$ GeV
$\Delta R(\ell j) > 1.5$
$ \vec{p}_T(\ell_1) - \vec{p}_T(\ell_2)  > 150$ GeV
$\cos(\delta\phi_{\ell\ell}) < -0.6$

**Table 3:** Additional selection cuts for channel  $2j\ell^\pm\ell^\pm\nu\nu$ .

The total cross section in femtobarns for the  $2j\ell^\pm\ell^\pm\nu\nu$  channel, with the full set of cuts in Tab. 1 and Tab. 3, as a function of the minimum invariant mass  $M_{cut}$  is shown in Tab. 4. In parentheses the results for the  $\mathcal{O}(\alpha_{EM}^6)$  contribution, which dominate the cross section, are reported. The distribution of  $M(\ell\ell)$  is presented on the right hand side of Fig. 1 which clearly demonstrates the good separation between the two scenarios obtained through the additional cuts. As expected the separation increases with increasing di-lepton invariant mass.

In Tab. 4 we also give the PBSM@95%CL for the two BSM scenarios. The corresponding normalized frequency for the three scenarios, as a function of the number of events, is reported in Fig. 2 for  $M_{cut} = 400$  GeV. The red curve refers to the probability distribution for a Higgs of 200 GeV while the green one refers to the SILH model and the blue one to the no-Higgs case. The dotted vertical line in the plot marks the 95% exclusion limit for the SM predictions.



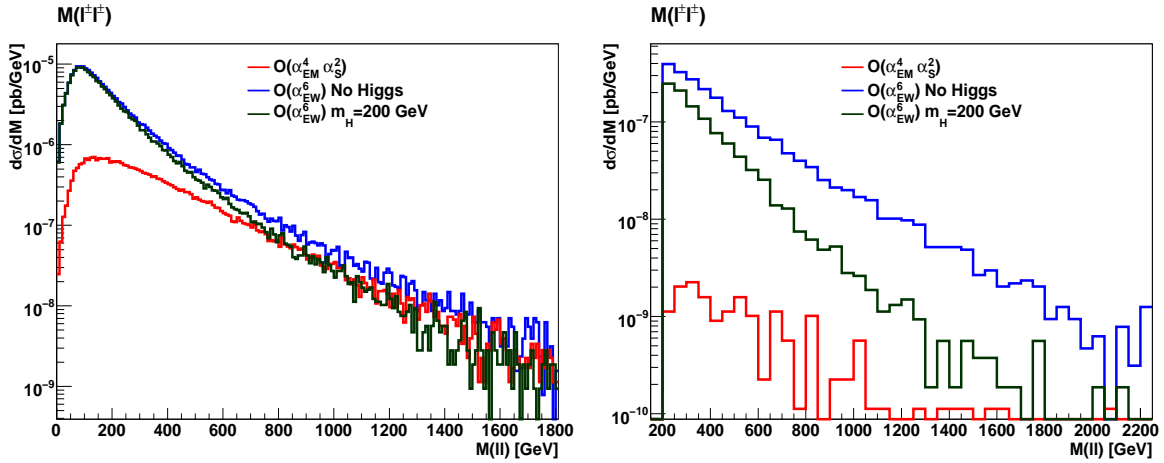


**Figure 1:**  $M(\ell\ell)$  distribution with acceptance cuts only, Tab. 1 (left) and after all additional selection cuts, Tab. 6 (right).

$M_{cut}$ (GeV)	no Higgs		SILH		$M_H = 200$ GeV
	$\sigma$ (fb)	PBSM	$\sigma$ (fb)	PBSM	$\sigma$ (fb)
200	.435(.431)	94.9%	.276 (.273)	39.1%	.206(.203)
300	.290(.288)	98.2%	.166 (.164)	42.3%	.114(.111)
400	.191(.189)	98.7%	.0977(.0958)	41.2%	.0629(.0609)
500	.129(.128)	98.7%	.0604(.0588)	34.4%	.0351(.0336)
600	.0886(.0876)	97.5%	.0385(.0375)	37.1%	.0194(.0183)
700	.0614(.0607)	96.6%	.0262(.0254)	42.3%	.0112(.0105)
800	.0438(.0432)	91.1%	.0184(.0178)	31.2%	.00701(.00640)

**Table 4:** Total cross section for the  $\ell^\pm\ell^\pm\nu\nu + 2j$  channel in femtobarns, with the full set of cuts in Tab. 1 and Tab. 3, as a function of the minimum dilepton invariant mass  $M_{cut}$  for the  $\ell^\pm\ell^\pm$  system. In parentheses the results for the  $\mathcal{O}(\alpha_{EM}^6)$  sample. We also show the PBSM probabilities. The result for  $M_{cut} = 400$  GeV which provides the best discrimination between the Higgsless and light Higgs scenario is highlighted.

The probability of an experiment to find a result incompatible with the SM at 95%CL assuming that the Higgsless model is realized in Nature is of the order of 99% for  $M_{cut} = 400$  GeV and decreases to about 90% for  $M_{cut} = 800$  GeV. Because of the absence of large backgrounds this channel has a discriminating power which is in fact quite high. The corresponding probabilities for the SILH model vary between 30% and 40%.

About 40(20) events are predicted for the Higgsless(SILH) scenario assuming our standard luminosity of  $L = 200 \text{ fb}^{-1}$  and  $M_{cut} = 400$  GeV, which provides the best discrimination between the Higgsless scenario and the SM.

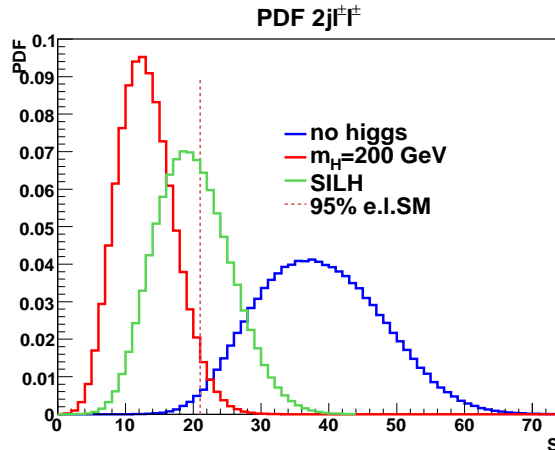


**Figure 2:** Probability distribution for no-Higgs, SILH and SM cases for the  $2j\ell^\pm\ell^\pm\nu\nu$  channel. The vertical line indicates the 95%CL for the SM.  $M_{cut} = 400$  GeV.

#### 4. The $2jZZ \rightarrow 2j\ell^+\ell^-\nu\bar{\nu}$ channel: two opposite-sign same-flavour leptons in the final state

This channel has been separated from the  $2jWW \rightarrow 2j\ell^+\ell^-\nu\bar{\nu}$  case using the di-lepton mass. If  $|M(\ell\ell) - M_Z| < 15$  GeV, the event is considered as produced by a  $ZZ$  intermediate state. Since the mass of the final state  $ZZ$  system cannot be fully reconstructed we estimate the center of mass energy of the vector boson scattering from their transverse mass:

$$M_T^2(ZZ) = [\sqrt{M_Z^2 + p_T^2(\ell\ell)} + \sqrt{M_Z^2 + p_{Tmiss}^2}]^2 - |\vec{p}_T(\ell\ell) + \vec{p}_{Tmiss}|^2 \quad (4.1)$$

The total cross section for the  $2jZZ \rightarrow 2j\ell^+\ell^-\nu\bar{\nu}$  channel with the acceptance cuts in Tab. 1 is presented in Tab. 5 as a function of the minimum  $M_{cut} = M_T^2(ZZ)$ . In parentheses the results for the  $\mathcal{O}(\alpha_{EM}^6)$  processes.

The  $M_T^2(ZZ)$  distribution, with acceptance cuts only, is presented on the left hand side of Fig. 3. The QCD background is much larger than in the channels discussed in Sect. 3. The contribution from top pair production is large, particularly at small transverse masses, even though we are requiring a lepton pair with an invariant mass in the neighborhood of the  $Z$  mass. This contribution rapidly fades at large  $M_T^2(ZZ)$  where the QCD processes without top are dominating. Moreover, since no requirement of large missing transverse momentum has been imposed, additional backgrounds at small transverse masses are generated by  $2jZ \rightarrow 2j\ell^+\ell^-$  production. We have not included this background contribution in our study since large  $p_{Tmiss}$  is demanded in our final analysis and this additional contribution is completely eliminated.

In order to sharpen the separation between the Standard Model results and those from alternative symmetry breaking scenarios we impose the additional cuts in Tab. 6.

The total cross section in femtobarns for the  $2jZZ \rightarrow 2j\ell^+\ell^-\nu\bar{\nu}$  channel, with the full set of cuts in Tab. 1 and Tab. 6, as a function of the minimum  $ZZ$  transverse mass  $M_{cut}$

$M_{cut}$ (GeV)	no Higgs	SILH	$M_H = 200$ GeV
	$\sigma$ (fb)	$\sigma$ (fb)	$\sigma$ (fb)
300	1.84 (.607)	1.73 (.494)	1.70(.464)
400	.675 (.319)	.578 (.222)	.544(.187)
500	.363 (.197)	.288 (.122)	.262(.0962)
600	.223 (.134)	.161 (.0727)	.140(.0515)
700	.143 (.0952)	.0947(.0466)	.0781(.0300)
800	.0926(.0686)	.0553(.0313)	.0426(.0186)
900	.0646(.0515)	.0341(.0210)	.0251(.0120)

**Table 5:** Total cross section for the  $(ZZ)\ell^+\ell^-\nu\nu + 2j$  channel after generation cuts, Tab. 1. In parentheses the results for the  $\mathcal{O}(\alpha_{EM}^6)$  sample.

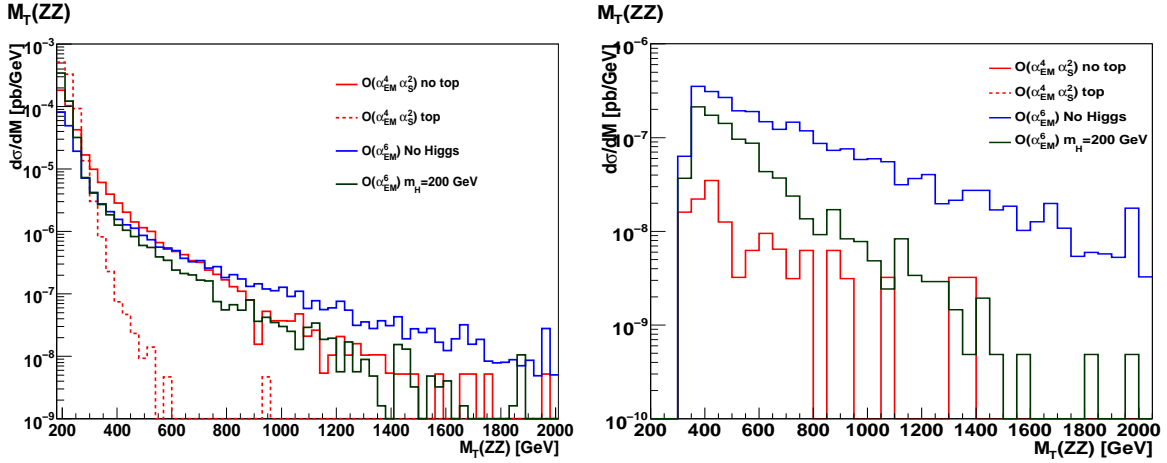


**Figure 3:** ZZ transverse mass distribution with initial cuts, Tab. 1 (left) and adding extra cuts, Tab. 6 (right).

is shown in Tab. 7. In parentheses the results for the  $\mathcal{O}(\alpha_{EM}^6)$  contribution. The PBSM probabilities are also given.

The  $M_T^2(ZZ)$  distribution, with the full set of cuts, is presented on the right hand side of Fig. 3. The  $\mathcal{O}(\alpha_{EM}^4 \alpha_S^2)$  background has been sharply reduced while increasing the separation between the Higgsless and light Higgs scenarios. The top related background has been totally suppressed.

The probability distribution for the three scenarios is reported in Fig. 4 for  $M_T(ZZ)_{cut} = 600$  GeV. The red curve refers to a Higgs of 200 GeV while the green one refers to the SILH model and the blue one to the no-Higgs case. The dotted vertical line in the plot marks the 95% exclusion limit for the SM predictions. The probability of an

$\Delta\eta(jj) > 4.5$
$M(jj) > 800$ GeV
$\Delta\eta(\ell j) > 1.3$
$p_{Tmiss} > 120$ GeV
$ \vec{p}_T(\ell^+\ell^-) - \vec{p}_T^{miss}  > 290$ GeV
$p_T(\ell^+\ell^-) > 120$ GeV
$\eta(j) > 1.9$

**Table 6:** Selection cuts for channel  $(ZZ)\ell^+\ell^-\nu\nu + 2j$ .

experiment to find a result incompatible with the SM at 95%CL assuming that the Higgsless model is realized in Nature is of the order of 98% for  $M_{cut} = 600$  GeV and does not vary significantly over the range considered in Tab. 7. The corresponding probabilities for the SILH model vary between 30% and 45%.

$M_{cut}$ (GeV)	no Higgs		SILH		$M_H = 200$ GeV
	$\sigma(\text{fb})$	PBSM	$\sigma(\text{fb})$	PBSM	$\sigma(\text{fb})$
300	.143(.136)	94.6%	.0770(.0700)	31.5%	.0540(.0470)
400	.120(.115)	96.1%	.0614(.0564)	36.2%	.0396(.0345)
500	.0887(.0860)	97.5%	.0396(.0369)	39.8%	.0214(.0187)
600	.0691(.0668)	98.4%	.0268(.0246)	44.3%	.0118(.00957)
700	.0547(.0533)	97.0%	.0186(.0171)	32.0%	.00697(.00555)
800	.0410(.0401)	94.6%	.0145(.0136)	33.2%	.00463(.00368)
900	.0327(.0321)	94.3%	.00991(.00927)	31.9%	.00300(.00236)

**Table 7:** Total cross section for the  $(ZZ)\ell^+\ell^-\nu\nu + 2j$  channel in femtobarns, with the full set of cuts in Tab. 1 and Tab. 6, as a function of the minimum transverse mass  $M_T(ZZ)_{cut}$ . In parentheses the results for the  $\mathcal{O}(\alpha_{EM}^6)$  sample. The PBSM@95%CL are also shown.

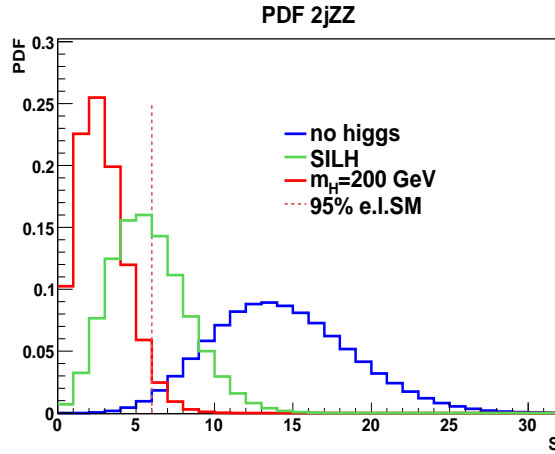


**Figure 4:** Probability distribution for the no-Higgs, SILH and SM cases for the  $2jZZ \rightarrow 2j\ell^+\ell^-\nu\bar{\nu}$  channel. The vertical line indicates the 95%CL for the SM.  $M_{cut} = 600$  GeV.

## 5. The $2jW^+W^- \rightarrow 2j\ell^+\ell^-\nu\bar{\nu}$ channel: two opposite-sign leptons in the final state

The total cross section for the  $2jW^+W^- \rightarrow 2j\ell^+\ell^-\nu\bar{\nu}$  channel, with the acceptance cuts in Tab. 1, is shown in Tab. 8 as a function of the minimum  $\ell\ell$  invariant mass. As usual, in parentheses we show the results for the  $\mathcal{O}(\alpha_{EM}^6)$  processes. This process has the largest production rate among all channels considered in this paper, however the QCD background is much larger than the electroweak part.

$M_{cut}$ (GeV)	no Higgs	SILH	$M_H = 200$ GeV
	$\sigma(\text{fb})$	$\sigma(\text{fb})$	$\sigma(\text{fb})$
250	111 (6.84)	111 (6.55)	110 (6.46)
300	70.0(4.65)	69.7(4.42)	69.7(4.35)
400	29.7(2.32)	29.5(2.11)	29.5(2.12)
500	13.5(1.24)	13.4(1.14)	13.4(1.13)
600	6.69(.713)	6.62(.643)	6.60(.627)
700	3.55(.440)	3.49(.376)	3.47(.362)
800	1.92(.274)	1.88(.236)	1.87(.225)

**Table 8:** Total cross section for the  $(W^+W^-)\ell^+\ell^-\nu\nu + 2j$  channel after initial cuts, Tab. 1 in function of the minimum  $\ell\ell$  invariant mass,  $M(\ell\ell)$ . In parentheses the results for the  $\mathcal{O}(\alpha_{EM}^6)$  sample.

The  $M(\ell\ell)$  distribution, with acceptance cuts only, is presented on the left hand side of Fig. 5.  $t\bar{t}$  production is very important at this level, and the usual way to suppress it, by requiring  $M(Wj)$  out of the top nominal mass window, is not applicable because of the impossibility to reconstruct the  $W$  mass. Instead we require the mass of all lepton-jet pairs to be larger than the top mass. Another important source of background is represented by EW top-production which contributes equally to the Higgsless and to the light Higgs scenarios. Indeed the two results are hardly distinguishable at this stage.

The relatively high signal rate and the large background allow and require harder cuts than in all previous cases. The additional selection requirements are shown in Tab. 9

The total cross section in femtobarns for the  $(W^+W^-)\ell^+\ell^-\nu\nu + 2j$  channel, with the full set of cuts in Tab. 1 and Tab. 9, as a function of the minimum di-lepton invariant mass  $M_{cut}$  is shown in Tab. 10. In parentheses the results for the  $\mathcal{O}(\alpha_{EM}^6)$  contribution. The PBSM probabilities are also presented.

The di-lepton mass distribution, with the full set of cuts, is presented on the right hand side of Fig. 5. The  $\mathcal{O}(\alpha_{EM}^4\alpha_s^2)$  background is now very small while the separation between the Higgsless and light Higgs scenarios is clearly visible.

The probability distribution for the three scenarios is reported in Fig. 6 for  $M(\ell\ell)_{cut} = 500$  GeV. The probability of an experiment to find a result incompatible with the SM at 95%CL assuming that the Higgsless model is realized in Nature is between 80 and 90% for  $250 \text{ GeV} < M_{cut} < 700 \text{ GeV}$ . For the SILH model the corresponding probabilities lie between 24 and 35%.

$M(jj) > 1000 \text{ GeV}$
$\Delta\eta(jj) > 4.8$
$ \eta(\ell)  < 2.00$
$p_T(\ell) > 40 \text{ GeV}$
$\max \eta(j)  > 2.5$
$ \eta(j)  > 1.3$
$E(j) > 180 \text{ GeV}$
$\Delta\eta(\ell j) > 0.8$ (and $\Delta R(\ell j) > 1$ )
$M(\ell j) > 180 \text{ GeV}$
$ \vec{p}_T(\ell^+) - \vec{p}_T(\ell^-)  > 220 \text{ GeV}$
$\cos(\delta\phi_{\ell\ell}) < -0.6$

**Table 9:** Additional selection cuts for the  $2jW^+W^- \rightarrow 2j\ell^+\ell^-\nu\nu$  channel.

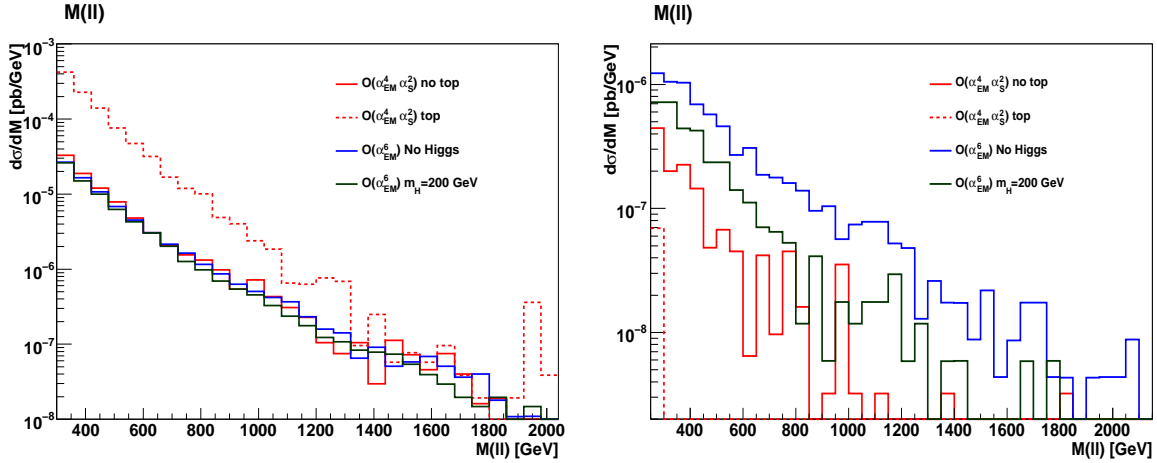


**Figure 5:** Di-lepton mass distribution with initial cuts, Tab. 1 (left) and adding extra cuts, Tab. 9 (right).

$M_{cut}$ (GeV)	no Higgs		SILH		$M_H = 200$ GeV
	$\sigma$ (fb)	PBSM	$\sigma$ (fb)	PBSM	$\sigma$ (fb)
250	.425(.354)	82.2%	.290(.219)	23.9%	.241(.170)
300	.337(.292)	85.6%	.224(.179)	26.3%	.179(.134)
400	.212(.188)	88.5%	.131(.107)	26.3%	.100 (.0765)
500	.139(.125)	90.8%	.0841(.0700)	35.3%	.0577(.0435)
600	.0968(.0883)	89.8%	.0533(.0448)	29.6%	.0332(.0247)
700	.0696(.0635)	89.5%	.0353(.0292)	29.1%	.0217(.0156)
800	.0500(.0466)	83.3%	.0243(.0210)	23.0%	.0131(.00970)

**Table 10:** Total cross section for the  $2jW^+W^- \rightarrow 2j\ell^+\ell^-\nu\nu$  channel in femtobarns, with the full set of cuts in Tab. 1 and Tab. 9, as a function of the minimum di-lepton invariant mass  $M(\ell\ell)_{cut}$ . In parentheses the results for the  $\mathcal{O}(\alpha_{EM}^6)$  sample. The PBSM probabilities are given in the third and fifth column.

## 6. The $2j4\ell$ channel

Contrary to all reaction discussed above, in the  $2j4\ell$  channel the mass of the final state vector boson pair can be directly measured to a high precision. It is presented here for completeness despite its small rate and statistical discriminating power.

The QCD contribution is small already at generation level. However, for a luminosity of  $L = 200 \text{ fb}^{-1}$  the difference between the number of events expected for an infinite mass Higgs and a light one is of the order the statistical uncertainty for the  $\mathcal{O}(\alpha_{EM}^4 \alpha_S^2)$  contribution and no meaningful separation between the two cases can be obtained. Only a minimum set of additional cuts can be applied in order to have at least a handful of events for  $L = 200 \text{ fb}^{-1}$ . This channel could clearly profit from higher luminosities. The additional selection cuts are shown in Tab. 11.

The cross section after these extra cuts is presented in Tab. 12 as a function of the

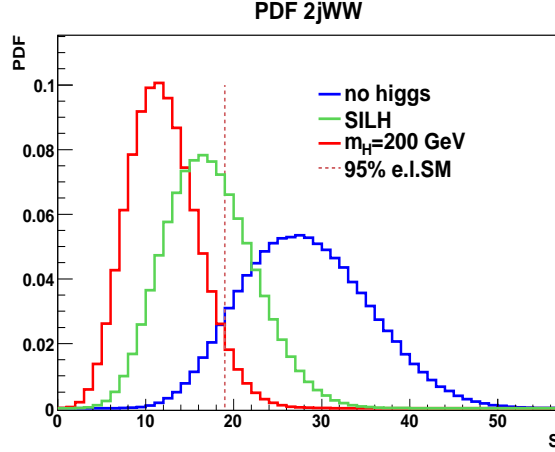


**Figure 6:** Probability distribution for the no-Higgs, SILH and SM cases for the  $2jW^+W^- \rightarrow 2j\ell^+\ell^-\nu\bar{\nu}$  channel. The vertical line indicates the 95%CL for the SM.  $M_{cut} = 500$  GeV.

minimum  $ZZ$  mass. In parentheses the results for the  $\mathcal{O}(\alpha_{EM}^6)$  sample. We also show the PBSM@95%CL for the standard  $L = 200 \text{ fb}^{-1}$ .

$M_{cut}$ (GeV)	no Higgs		SILH		$M_H = 200 \text{ GeV}$
	$\sigma(\text{ab})$	PBSM	$\sigma(\text{ab})$	PBSM	$\sigma(\text{ab})$
300	51.8(41.6)	35.6%	36.1(26.0)	8.4%	31.6(21.5)
400	44.7(36.7)	40.7%	30.1(22.1)	10.3%	25.5(17.5)
500	35.6(30.1)	41.8%	22.8(17.3)	10.5%	18.4(12.9)
600	28.2(24.2)	34.1%	17.2(13.2)	7.0%	13.5(9.45)
700	22.2(19.5)	29.3%	12.8(10.0)	5.3%	9.64(6.93)
800	17.8(15.8)	29.1%	9.79(7.82)	5.4%	7.09(5.12)
900	14.0(12.6)	31.0%	7.38(6.05)	6.7%	5.19(3.87)

**Table 12:** Total cross section for the  $4\ell + 2j$  channel in attobarns, with the full set of cuts in Tab. 1 and Tab. 11, as a function of the minimum invariant mass  $M_{cut}$  for the  $4\ell$  system. In parentheses the results for the  $\mathcal{O}(\alpha_{EM}^6)$  sample. Also shown are the PBSM probabilities.

The probability distribution of the discriminant  $S$  for the three scenarios is reported in Fig. 7 for  $M_{cut} = 500$  GeV with the full set of cuts in Tab. 1 and Tab. 11.

As reported in Tab. 12, the probability of an experiment to find a result incompatible with the SM at 95%CL assuming that the Higgsless model is realized in Nature is of the order of 42% for  $M_{cut} = 500$  GeV and decreases to about 30% for  $M_{cut} = 700$  GeV. For the SILH model the PBSM@95%CL is only about 10% at most, for  $M_{cut} = 500$  GeV.

For  $L = 200 \text{ fb}^{-1}$  and summing over all final states, the expected total rates are of the order of  $4 \div 8$  events for the Higgsless case.

$M(jj) > 800 \text{ GeV}$
$p_T(Z) > 100 \text{ GeV}$
$\Delta R(Zj) > 1$
$\cos(\delta\phi_{ZZ}) < -0.4$

**Table 11:** Additional selection cuts for the  $2j4\ell$  channel.

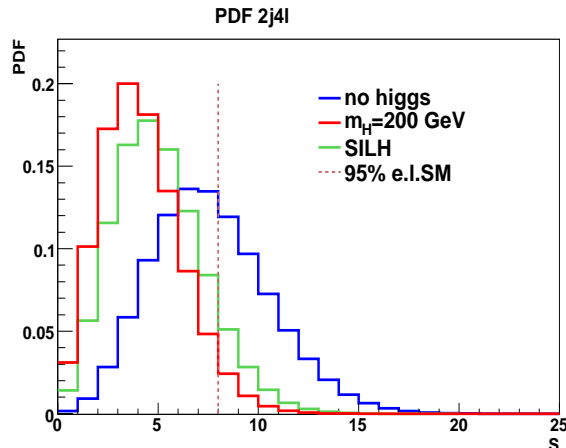


**Figure 7:** Probability distribution for the no-Higgs, SILH and SM cases for the  $2j4l$  channel. The vertical line indicates the 95%CL for the SM.  $M_{cut} = 500$  GeV.

## 7. Combining all channels

In this section we derive the probability that, assuming that either the Higgsless scenario or the instance of SILH model we have considered is realized in Nature, the results of the measurements of the seven channels  $2j\ell^\pm\ell^\pm\nu\nu$ ,  $2jZZ \rightarrow 2j\ell\nu\ell\nu$ ,  $2jWW \rightarrow 2j\ell\nu\ell\nu$ ,  $2j4l$ ,  $4j\ell\nu$ ,  $4j\ell\ell$  and  $2j3\ell\nu$  at the LHC yield results which are outside the 95% probability region for the SM.

Tab. 13 shows the number of expected events for the reactions in which the  $VV$  mass can be reconstructed. The data for  $4j\ell\nu$  production are taken from Ref. [27] while those for  $4j\ell^+\ell^-$  and  $2j\ell^+\ell^-\ell'\nu$  are from Ref. [28] to which we refer for more details. Tab. 14 instead shows the number of expected events for the channels in which direct reconstruction of the vector boson pair mass is impossible. In both instances the assumed integrated luminosity is  $200 \text{ fb}^{-1}$ . In each case the prediction corresponds to the value of  $M_{cut}$  which gives the best PBSM@95%CL. These values are highlighted in Tables 4, 7, 10 and 12 for the reactions described in detail in this paper. For the remaining channels  $M_{cut}$  has been set to 600 GeV.

For a given number of events for each channel,  $k_1, k_2, \dots, k_n$  with corresponding mean values  $\lambda_1, \lambda_2, \dots, \lambda_n$ , which we will refer to collectively as  $\vec{k}$  and  $\vec{\lambda}$ , the standard likelihood ratio in Eq.(2.3) can be expressed as  $Q(\vec{k}; \vec{\lambda}_{BSM}, \vec{\lambda}_{SM}) = P(\vec{k}, \vec{\lambda}_{BSM})/P(\vec{k}, \vec{\lambda}_{SM})$

The procedure we have employed so far and in Ref. [28] to evaluate the PBSM becomes cumbersome when too many channels have to be considered and the dimensionality of the integrals in Eqs.(2.4, 2.5) becomes large. Therefore for the combination of all results we have resorted to the variable  $-2\ln Q$ . From the one dimensional probability distribution of  $-2\ln Q$  the 95%CL and 99.7%CL limits for the SM can be easily determined.

In the following we will first combine separately the first three channels, in which the invariant mass of the  $VV$  pair cannot be reconstructed, and the last four, in which the  $VV$  mass can be directly measured. Later we will proceed to a full combination.



	S(noHiggs)	S(SILH)	S( $m_H = 200$ GeV)	B $\mathcal{O}(\alpha_{EM}^2 \alpha_S^4)$
$4j\ell\nu$	473.6	281.6	210.4	1956.
$4j\ell^+\ell^-$	61.6	30.4	19.38	220.
$2j\ell^+\ell^-\ell'\nu$	10.8	5.4	3.4	–
$2j\ell^+\ell^-\ell^+\ell^-$	7.12	4.56	3.68	–

**Table 13:** Number of events expected for  $L = 200fb^{-1}$  for the channels in which the  $VV$  mass can be reconstructed. The cuts for the first three reactions are described in [27] and [28]. The cuts for the  $2j4\ell$  channel are discussed in Sect. 6.  $M_{cut}$  is chosen in such a way that the best PBSM@95%CL for each channel is obtained.

	S(noHiggs)	S(SILH)	S( $m_H = 200$ GeV)
$2j\ell^\pm\ell^\pm\nu\nu$	38.2	19.54	12.58
$2jZZ \rightarrow \ell^+\ell^-\nu\nu$	13.82	5.36	2.36
$2jW^+W^- \rightarrow \ell^+\ell^-\nu\nu$	27.8	16.82	11.54

**Table 14:** Number of events expected for  $L = 200fb^{-1}$  for the channels in which the  $VV$  mass cannot be reconstructed.  $M_{cut}$  is chosen in such a way that the best PBSM@95%CL for each channel is obtained.

The probability  $P(\vec{k}, \vec{\lambda})$  depends on the correlations between channels. In our simplified approach in which only statistical and theoretical errors are accounted for, only the uncertainties which are related to theory are correlated. Statistical errors in each channel are independent.

As a first step, we assume each channel to be subject to an independent theoretical error which is implemented by smearing the mean value for each channel separately and then combining the smeared channels. The corresponding probability, for the simple case in which the  $\mathcal{O}(\alpha_{EM}^2 \alpha_S^4)$  background is absent, is given by:

$$P_U(\vec{k}; \vec{\lambda}) = \prod_i \int dx_i \rho(x_i) \mathcal{P}(k_i, (1+x_i)\lambda_i) \quad (7.1)$$

where  $\mathcal{P}(k, \lambda)$  is the standard Poisson distribution with mean  $\lambda$  and

$$\rho(x) = \begin{cases} \frac{1}{2 \times 0.3} & \text{if } |x| < 0.3 \\ 0 & \text{otherwise} \end{cases} \quad (7.2)$$

models the (flat) theoretical uncertainty.

Combining separately the two set of channels we obtain the probabilities to exclude the SM at 95%CL and at 99.7%CL shown in Tab. 15.

The hypothesis that the theoretical errors in each channel are independent may underestimate the actual uncertainty. The dominant production mechanisms are the same for all channels and therefore it is likely that both pdf and scale uncertainties are fully correlated between channels. Assuming this to be the case for the total theoretical uncertainty, the average values of each channel which enter the combination must be shifted by a common factor and the corresponding probability  $P_C$  can be expressed as

uncorrelated error				
	non-reconstructable		reconstructable	
	NOH	SILH	NOH	SILH
95%CL	99.9994 %	77.8776 %	99.9665%	53.2053%
99.7%CL	99.9824 %	43.0707%	99.3734%	19.0392%

**Table 15:** Probability to exclude the SM with different confidence levels, for different strong alternative scenarios combining the three non-reconstructable channels ( $2j\ell^\pm\ell^\pm\nu\nu$ ,  $ZZ \rightarrow 2j\ell\nu\ell\nu$  and  $WW \rightarrow 2j\ell\nu\ell\nu$ ), and the four reconstructable ones ( $4j\ell\nu$ ,  $4j\ell\ell$ ,  $2j3\ell\nu$  and  $2j4\ell$ ). Theoretical errors are assumed to be uncorrelated as in Eq.(7.1).

strongly-correlated error				
	non-reconstructable		reconstructable	
	NOH	SILH	NOH	SILH
95%CL	99.9862 %	66.1751%	99.3957%	45.2529%
99.7%CL	99.6529 %	35.5119%	94.7209%	17.4008%

**Table 16:** Probability to exclude the SM with different confidence levels, for different strong alternative scenarios combining the three non-reconstructable channels ( $2j\ell^\pm\ell^\pm\nu\nu$ ,  $ZZ \rightarrow 2j\ell\nu\ell\nu$  and  $WW \rightarrow 2j\ell\nu\ell\nu$ ), and the four reconstructable ones ( $4j\ell\nu$ ,  $4j\ell\ell$ ,  $2j3\ell\nu$  and  $2j4\ell$ ). Theoretical errors are assumed to be fully correlated as in Eq.(7.3).

$$P_C(\vec{k}; \vec{\lambda}) = \int dx \rho(x) \prod_i \mathcal{P}(k_i, (1+x)\lambda_i). \quad (7.3)$$

The PBSM@95%CL and PBSM@99.7%CL in case of complete correlation between theoretical errors are shown in Tab. 16. Comparing Tab. 16 with Tab. 15, it is clear that dropping the hypothesis of independent theoretical errors degrades little the overall probability. Within the present theoretical framework it remains certain that the no-Higgs case would be distinguished from the SM case. In the SILH model the PBSM@95%CL drops from 78% to 66% for the non-reconstructable channels and from 53% to 45% for the reconstructable ones.

The non-reconstructable channels presented here, independently of the detailed treatment of the theoretical uncertainty, provide a better discrimination between the SM and the BSM scenarios, despite their low rates, than those in which the invariant mass of the boson pair can be measured. This is clearly related to the absence of huge QCD backgrounds, which are instead present in the  $V + 4j$  channels. The statistical uncertainties of these background are large and spoil the significance of the corresponding channels even when the backgrounds are assumed to be measured from the sidebands of the weak boson peak in the mass distribution of the two central jets and then subtracted as proposed in Refs. [27, 28].

The distribution of  $-2 \ln Q$ , for the combination of all seven channels, in the Higgsless and SILH scenarios with our standard luminosity are shown in the top row of Fig. 8. In the bottom row of Fig. 8 we present the distributions for the Higgsless case with a luminosity

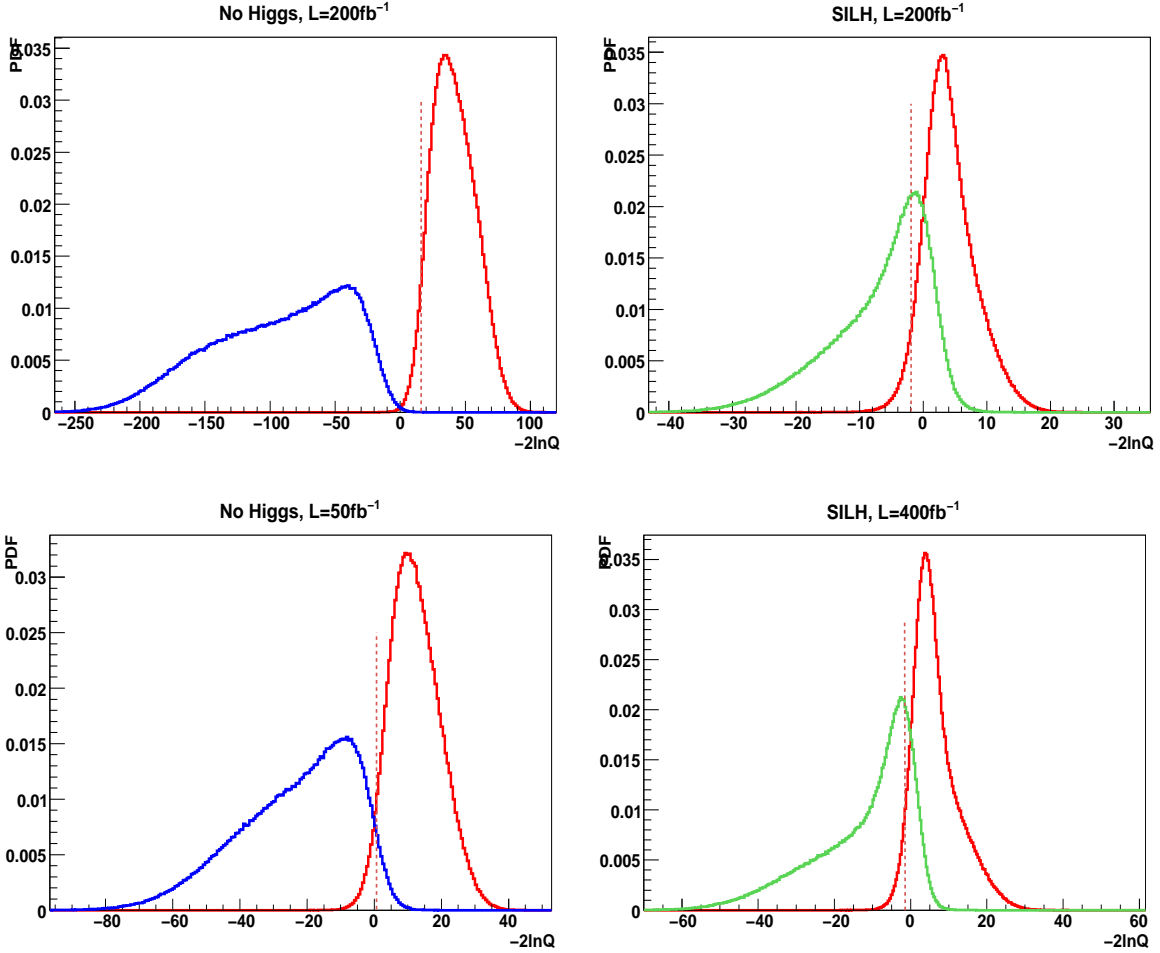


**Figure 8:** Combination of all the seven channels using  $-2 \ln Q$  for the no-Higgs and SILH cases using strongly correlated theoretical errors. In the bottom plots an integrated luminosity of  $L = 50 \text{ fb}^{-1}$  is assumed for the no-Higgs scenario and of  $L = 400 \text{ fb}^{-1}$  for the SILH case. For the no-Higgs analysis at  $L = 50 \text{ fb}^{-1}$  we have used the lowest mass cut for each channel in order to increase the number of events at this luminosity. Hence in this case  $M_{cut} = 200, 300, 250, 300 \text{ GeV}$  for the  $2j\ell^\pm\ell^\pm\nu\nu$ ,  $ZZ \rightarrow 2j\ell\nu\nu$ ,  $WW \rightarrow 2j\ell\nu\nu$  and  $2j4\ell$  channel respectively. For the remaining channels  $M_{cut}$  has been kept at  $600 \text{ GeV}$ .

total combination				
	NOH	SILH	NOH( $L = 50 \text{ fb}^{-1}$ )	SILH( $L = 400 \text{ fb}^{-1}$ )
95%CL	99.9997%	69.3829%	96.4943%	80.2009%
99.7%CL	99.9562%	42.1324%	84.1348%	56.4486%

**Table 17:** Statistical combination of all seven channels. Also shown are the results using an integrated luminosity of  $L = 50 \text{ fb}^{-1}$  for the no-Higgs and of  $L = 400 \text{ fb}^{-1}$  for the SILH scenario. For the no-Higgs analysis we have used the lowest mass cut for each channel in order to increase the number of events at this luminosity.

of  $50 \text{ fb}^{-1}$  and for the SILH model with  $L = 400 \text{ fb}^{-1}$ . In all cases theoretical errors are treated as fully correlated. For the no-Higgs case at  $L = 50 \text{ fb}^{-1}$  we have adopted the

lowest invariant mass cut reported in Tables 4, 7, 10 and 12 for the reactions discussed in this paper, in order to increase the number of events at this luminosity. Explicitly,  $M_{cut} = 200, 300, 250, 300$  GeV for the  $2j\ell^\pm\ell^\pm\nu\nu$ ,  $ZZ \rightarrow 2j\ell\nu\ell\nu$ ,  $WW \rightarrow 2j\ell\nu\ell\nu$  and  $2j4\ell$  channel respectively. For the remaining channels  $M_{cut}$  has been kept at 600 GeV. The corresponding PSM@95%CL and PSM@99.7%CL are given in Tab. 17. Assuming an integrated luminosity of  $200 \text{ fb}^{-1}$  the PSM@95%CL for the SILH case is about 69% which increases to 80% if the luminosity is doubled. The corresponding figures for the PSM@99.7%CL are 42% and 56% respectively. The probability to distinguish at 95%CL the no-Higgs case from the light Higgs picture with a reduced luminosity of  $L = 50 \text{ fb}^{-1}$  remains above 95%.

These results suggest that the no-Higgs scenario can be disproved with a rather modest luminosity. This implies that any model which predicts vector vector scattering rates larger than those in the no-Higgs case can be disproved or verified with the same luminosity.

Our conclusions for the SILH framework are less optimistic. Clearly a substantial increase in luminosity and a combination of the results obtained by ATLAS and CMS are highly desirable. Furthermore, it should be recalled that the particular instance of SILH model we have discussed is a rather extreme case and that for smaller values of  $c_{H\xi}$  results even closer to the SM ones are expected.

## 8. Conclusions

We have examined in detail at parton level the processes  $2\ell 2\nu 2j$  and  $4\ell 2j$ ,  $\ell = \mu, e$  including all irreducible backgrounds contributing to these six parton final states. We have considered three scenarios: a light Higgs SM framework with  $M_H = 200$  GeV, one instance of the SILH models and an infinite mass Higgs scenario in order to determine whether the two BSM models can be distinguished from the SM at the LHC using boson-boson scattering. Because of the absence of large QCD backgrounds, the non-reconstructable channels presented here, provide a better discrimination between the SM and the BSM scenarios despite their low rates than those in which the invariant mass of the boson pair can be measured.

The results for the channels discussed above have been combined with those obtained in Ref. [27] for  $4j\ell\nu$  production and those obtained in Ref. [28] for  $4j\ell^+\ell^-$  and  $2j3\ell\nu$ . We have estimated the total probability, in the two BSM scenarios, of finding a result outside the 95% probability range in the Standard Model. This probability turns out to be essentially 100% for the Higgsless case and 69% for the SILH model. These probabilities correspond to an integrated luminosity of  $L = 200 \text{ fb}^{-1}$  and to the sum of all electron and muon channels.

## Acknowledgments

A.B. wishes to thank the Dep. of Theoretical Physics of Torino University for support. This work has been supported by MIUR under contract 2006020509 004 and by the Eu-

## References

- [1] Proceedings of the Large Hadron Collider Workshop, Aachen 1990, CERN Report 90-10, G. Jarlskog and D. Rein (eds.).
- [2] A. Djouadi, *The Anatomy of Electro-Weak Symmetry Breaking. Tome I: The Higgs in the Standard Model*, [arXiv:hep-ph/0503172].
- [3] ATLAS Collaboration, *Detector and Physics Performance Technical Design Report*, Vols. 1 and 2, CERN-LHCC-99-14 and CERN-LHCC-99-15.
- [4] K.A. Assamagan, M. Narain, A. Nikitenko, M. Spira, D. Zeppenfeld (conv.) *et al.*, Report of the Higgs Working Group, Proceedings of the Les Houches Workshop on “Physics at TeV Colliders”, 2003, [arXiv:hep-ph/0406152].
- [5] CMS Collaboration, *Technical Design Report*, Vols. 1 and 2, CERN/LHCC 2006-001 and CERN/LHCC 2006-021.
- [6] M.S. Chanowitz, *Strong WW scattering at the end of the 90's: theory and experimental prospects*. In *Zuoz 1998, Hidden symmetries and Higgs phenomena* 81-109. [arXiv:hep-ph/9812215]
- [7] D. B. Kaplan and H. Georgi, Phys. Lett. B **136** (1984) 183.
- [8] N. Arkani-Hamed, A. G. Cohen and H. Georgi, Phys. Lett. B **513** (2001) 232.
- [9] N. Arkani-Hamed, A. G. Cohen, E. Katz and A.E. Nelson, JHEP 0207, 034 (2002), [arXiv:hep-ph/0206021].
- [10] N. S. Manton, Nucl. Phys. B **158** (1979) 141; Y. Hosotani, Annals Phys. **190** (1989) 233.
- [11] C. Csaki, C. Grojean and H. Murayama, Phys. Rev. D **67** (2003) 085012; C. A. Scrucca, M. Serone and L. Silvestrini, Nucl. Phys. B **669** (2003) 128.
- [12] K. Agashe, R. Contino and A. Pomarol, Nucl. Phys. B **719** (2005) 165.
- [13] S. Chang, JHEP 0312, 057 (2003), [arXiv:hep-ph/0306034].
- [14] G.F. Giudice, C. Grojean, A. Pomarol, R. Rattazzi, JHEP 0706:045,2007, [arXiv:hep-ph/0703164].
- [15] T. Appelquist and C.W. Bernard, *Phys. Rev.* **D22** (1980) 200; A.C. Longhitano, *Phys. Rev.* **D22** (1980) 1166; A.C. Longhitano, *Nucl. Phys.* **B188** (1981) 118; T. Appelquist and G.H. Wu, *Phys. Rev.* **D48** (1993) 3235(1993) [hep-ph/9304240].
- [16] R. Contino, T. Kramer, M. Son and R. Sundrum, JHEP **0705** (2007) 074.
- [17] R. Barbieri, B. Bellazzini, V.S. Rychkov, A. Varagnolo, Phys.Rev.D76:115008,2007, arXiv:0706.0432 [hep-ph].

- [18] M.J. Duncan, G.L. Kane and W.W. Repko, *Nucl. Phys.* **B272** (1986) 517; D.A. Dicus and R. Vega, *Phys. Rev. Lett.* **57** (1986) 1110; R.N. Cahn, S.D. Ellis, R. Kleiss and W.J. Stirling, *Phys. Rev. D* **35** (1987) 1626; V. Barger, T. Han and R. Phillips, *Phys. Rev. D* **37** (1988) 2005 and *D* **36** (1987) 295; R. Kleiss and J. Stirling, *Phys. Lett.* **200B** (1988) 193; V. Barger *et al.*, *Phys. Rev. D* **42** (1990) 3052; V. Barger *et al.*, *Phys. Rev. D* **44** (1991) 1426; V. Barger *et al.*, *Phys. Rev. D* **46** (1992) 2028; D. Froideveaux, in Ref. [1] Vol II, p. 444; M. H. Seymour, in Ref. [1] Vol II, p. 557; U. Baur and E.W.N. Glover, *Phys. Lett.* **B252** (1990) 683; D. Dicus, J. Gunion and R. Vega, *Phys. Lett.* **B258** (1991) 475; D. Dicus, J. Gunion, L. Orr and R. Vega, *Nucl. Phys.* **B377** (1991) 31; J. Bagger *et al.*, *Phys. Rev.* **D49** (1994) 1246; V. Barger, R. Phillips and D. Zeppenfeld, *Phys. Lett.* **B346** (1995) 106; J. Bagger *et al.*, *Phys. Rev.* **D52** (1995) 3878; K. Iordanidis and D. Zeppenfeld, *Phys. Rev.* **D57** (1998) 3072; R. Rainwater and D. Zeppenfeld, *Phys. Rev.* **D60** (1999) 113004; erratum *ibid* **D61** (2000) 099901.
- [19] E. Accomando, A. Ballestrero, S. Bolognesi, E. Maina and C. Mariotti, *JHEP* **0603** (2006) 093 [arXiv:hep-ph/0512219].
- [20] E. Accomando, A. Ballestrero, A. Belhouari and E. Maina, *Phys. Rev. D* **75** (2007) 113006 [arXiv:hep-ph/0603167].
- [21] G. Bevilacqua, in F. Ambroglini *et al.*, *Proceedings of the Workshop on Monte Carlo's, Physics and Simulations at the LHC PART II*, Frascati, Italy.
- [22] K. Cheung, C. Chiang and T. Yuan, *Phys. Rev. D* **78**(2008)051701, arXiv:0803.2661 [hep-ph].
- [23] B. Jäger, C. Oleari and D. Zeppenfeld, *JHEP* **0607** (2006) 015, [hep-ph/0603177]; B. Jäger, C. Oleari and D. Zeppenfeld, *Phys. Rev. D* **73**:113006,2006, [hep-ph/0604200]; G. Bozzi, B. Jäger, C. Oleari and D. Zeppenfeld, *Phys. Rev. D* **75**:073004,2007, [hep-ph/0701105]; B. Jäger, C. Oleari and D. Zeppenfeld, *Phys. Rev. D* **80**:034022,2009, arXiv:0907.0580 [hep-ph].
- [24] K. Arnold *et al.*, *Comput. Phys. Commun.* **180**:1661,2009, arXiv:0811.4559 [hep-ph].
- [25] C.F. Berger *et al.*, arXiv:1009.2338 [hep-ph].
- [26] T. Han, D. Krohn, L.T. Wang and W. Zhu, *JHEP* **1003**:082,2010, arXiv:0911.3656 [hep-ph].
- [27] A. Ballestrero, G. Bevilacqua and E. Maina *JHEP* **05** (2009) 015, arXiv:0812.5084 [hep-ph].
- [28] A. Ballestrero, G. Bevilacqua, D. Buarque Franzosi and E. Maina *JHEP* **11** (2009) 126, arXiv:0909.3838 [hep-ph].
- [29] J. Bagger *et al.*, *Phys. Rev.* **D49** (1994) 1246; J. Bagger *et al.*, *Phys. Rev.* **D52** (1995) 3878.
- [30] Z. Sullivan and E.L. Berger, *Phys. Rev.* **74** (2006) 033008, Z. Sullivan and E.L. Berger, *Phys. Rev.* **78** (2008) 034030.
- [31] Bo Zhu *et al.*, arXiv:1010.5848 [hep-ex].
- [32] A. Ballestrero, A. Belhouari, G. Bevilacqua, V. Kashkan and E. Maina, *Comp. Phys. Commun.* **180** (2009) 401, arXiv:0801.3359 [hep-ph].
- [33] E. Accomando, A. Ballestrero, E. Maina, *JHEP* **0507** (2005) 016, [arXiv:hep-ph/0504009].
- [34] A. Ballestrero and E. Maina, *Phys. Lett.* **B350** (1995) 225, [arXiv:hep-ph/9403244].

- [35] A. Ballestrero, PHACT 1.0 - *Program for Helicity Amplitudes Calculations with Tau matrices* [arXiv:hep-ph/9911318] in *Proceedings of the 14th International Workshop on High Energy Physics and Quantum Field Theory (QFTHEP 99)*, B.B. Levchenko and V.I. Savrin eds. (SINP MSU Moscow), pg. 303.
- [36] J. Alwall *et al.*, A Standard format for Les Houches event files. Written within the framework of the MC4LHC-06 workshop: Monte Carlos for the LHC: A Workshop on the Tools for LHC Event Simulation (MC4LHC), Geneva, Switzerland, 17-16 Jul 2005, *Comp. Phys. Commun.* **176** (2007) 300, [arXiv:hep-ph/0609017].
- [37] CTEQ Coll.(H.L. Lai *et al.*) *Eur. Phys. J.* **C12** (2000) 375.
- [38] A. Ballestrero, D. Buarque Franzosi, E. Maina and L. Oggero, in preparation.
- [39] A.D. Martin, R.G. Roberts, W.J. Stirling and R.S. Thorne, *Eur. Phys. J.* **C28** (2003) 455, [hep-ph/0211080].
- [40] A.D. Martin, R.G. Roberts, W.J. Stirling and R.S. Thorne, *Eur. Phys. J.* **C35** (2004) 325, [hep-ph/0308087].
- [41] A. Kulesza and W.J. Stirling, *Phys. Lett.* **B475** (2000) 168, [hep-ph/9912232].
- [42] E. Maina, *JHEP* 09 (2009) 081, arXiv:0909.1586 [hep-ph].
- [43] J.R. Gaunt, C. Kom, A. Kulesza and W.J. Stirling, arXiv:1003.3953.